Ground States and Ionization Energies of Si_2H_6, Si_3H_8, Si_4H_{10}, and Si_5H_{12}

J. V. Ortiz*,† and J. W. Mintmire‡

Contribution from the Department of Chemistry, University of New Mexico, Albuquerque, New Mexico 87131, and Chemistry Division, Naval Research Laboratory, Washington, D.C. 20375. *Received December 9, 1987*

Abstract: Ab initio calculations are performed on the structures and vertical ionization energies of the title molecules. The ground-state calculations employ Hartree–Fock, double-ζ plus polarization geometry optimizations. Second-order perturbative correlation energies are also calculated. Electron propagator theory is employed for the vertical ionization energies. Energy differences between minima on the ground-state surface are quite small. Tetrasilane rotation barriers are in the neighborhood of 1 kcal/mol. Vertical ionization energies have a much larger dependence on rotations about single bonds. For tetrasilane, the experimental photoelectron spectrum represents a mixture of rotational minima. Good agreement with experiment is obtained for all the molecules. Simple molecular orbital ideas suffice to explain the conformational dependence of the spectra.

I. Introduction

Electronically saturated Si polymers are attracting attention because of the many interesting chemical and physical properties that they exhibit.[1] Absorbance in the ultraviolet by molecules with no π, d, or lone-pair electrons[2] stimulates investigation of their electronic structure. Bathochromic shifts attributed to order–disorder transitions of substituted polysilanes in solution suggest that absorption is strongly dependent on conformation.[3] ESR spectra of stable radical anions[4] and low-lying ionization energies[5] illustrate the delocalization of particle and hole states in these σ systems. Photochemical properties, such as self-developing photoresist behavior,[6] are also under study.

Theoretical work in this area has consisted of semiempirical calculations on large molecules and polymers or ab initio studies of small species. Semiempirical calculations have concentrated on spectra, structures, and barriers to rotation.[7] Several suggestions of the nature of the valence and conduction bands of polysilanes have been made from band calculations.[8] Relative energies of rotational isomers using empirical force fields have been calculated.[9] Few ab initio studies have been published on the electronic structure of any of these systems larger than disilane.[10]

Ab initio calculations on small silane chains are therefore needed to provide accurate bench marks of physical properties that can be used in effective force-field calculations on ground-state conformations or in parametrized calculations of spectra. Larger chains can be studied more reliably in this way. At the same time, a comparison of theoretical calculations against available experimental data for the small systems that ab initio theory can attack is necessary to confirm the validity of the theoretical model. The present calculations therefore concentrate on two aspects of small silanes. First, geometry optimization is used for obtaining accurate structures and relative energies of rotational isomers. Second, vertical ionization energy calculations, which can be compared with photoelectron spectra, disclose aspects of electronic structure that relate spectra to structure.

II. Methods

Hartree–Fock geometry optimizations are performed with the 3-21G* basis set.[11] There is ample evidence that this treatment, which includes d functions on the Si atoms, gives accurate geometries for Si-containing chains.[10] Studies of disilane with larger basis sets give no substantial improvements at the Hartree–Fock level, but the inclusion of d functions on the Si atoms is necessary.[12] At the optimum HF/3-21G* geometries, single-point Hartree–Fock and MBPT(2)[13] total energies are calculated with the 6-31G* basis. Electron propagator theory[14] (EPT) is used subsequently to calculate vertical ionization energies from the same structures. In EPT calculations the relaxation and correlation corrections to Koopmans's theorem[15] are contained in the energy-dependent self-energy, $\Sigma(E)$, of the Dyson equation.

$$G^{-1}(E) = G_0^{-1}(E) - \Sigma(E)$$

Table I. Si_2H_6 EPT/6-31G* Vertical Ionization Energies (eV)

	Koopmans	EPT(2)	EPT(3)	EPT(OVA)	exptl[5a,b]
$^2A_{1g}$	10.99	10.30	10.26	10.32	10.53
^2E_g	12.88	11.99	11.92	12.00	11.9, 12.1
^2E_u	13.62	12.74	12.68	12.75	12.73, 13.08

Table II. Si_2H_6 EPT/6-31+G* Vertical Ionization Energies (eV)

	Koopmans	EPT(2)	EPT(3)	EPT(OVA)	exptl[5a,b]
$^2A_{1g}$	11.05	10.34	10.32	10.37	10.53
^2E_g	12.93	12.03	11.97	12.04	11.9, 12.1
^2E_u	13.67	12.77	12.72	12.80	12.73, 13.08

† University of New Mexico.
‡ Naval Research Laboratory.

(1) (a) West, R.; Carberry, E. *Science (Washington, D.C.)* **1975**, *189*, 179. (b) West, R. *J. Organomet. Chem.* **1986**, *300*, 327.
(2) (a) Gilman, H.; Atwell, W. H.; Schwebke, G. L. *Chem. Ind. (London)* **1964**, 1063; *J. Organomet. Chem.* **1964**, *2*, 369. (b) Pitt, C. G. In *Homoatomic Rings, Chains and Macromolecules of Main Group Elements*; Rheingold, A. L., Ed.; Elsevier: Amsterdam, The Netherlands, 1977. (c) Rabolt, J. F.; Hofer, D.; Miller, R. D.; Fickes, G. N. *Macromolecules* **1986**, *19*, 611. (d) Ernst, C. A.; Allred, A. L.; Ratner, M. A. *J. Organomet. Chem.* **1979**, *178*, 119. (e) Allred, A. L.; Ernst, C. A.; Ratner, M. A. In *Homoatomic Rings, Chains and Macromolecules of Main Group Elements*; Rheingold, A. L., Ed.; Elsevier: Amsterdam, The Netherlands, 1977.
(3) (a) Miller, R. D.; Hofer, D.; Rabolt, J.; Fickes, G. N. *J. Am. Chem. Soc.* **1985**, *107*, 2172. (b) Harrah, L. A.; Zeigler, J. M. *J. Polym. Sci., Polym. Lett. Ed.* **1985**, *23*, 209. (c) Trefonas, P.; Damewood, J. R.; West, R.; Miller, R. D. *Organometallics* **1985**, *4*, 1318. (d) Trefonas, P.; West, R.; Miller, R. D.; Hofer, D. *J. Polym. Sci., Polym. Lett. Ed.* **1983**, *21*, 823.
(4) (a) Carberry, E.; West, R. *J. Organomet. Chem.* **1966**, *6*, 582. (b) West, R.; Indriksons, A. *J. Am. Chem. Soc.* **1972**, *94*, 6110. (c) West, R.; Kean, E. S. *J. Organomet. Chem.* **1975**, *96*, 323. (d) Carberry, E.; West, R.; Glass, G. E. *J. Am. Chem. Soc.* **1969**, *91*, 5446.
(5) (a) Bock, H.; Ensslin, W.; Feher, F.; Freund, R. *J. Am. Chem. Soc.* **1976**, *98*, 668. (b) Ensslin, W.; Bergmann, H.; Elbel, S. *J. Chem. Soc., Faraday Trans. 2* **1975**, *71*, 913. (c) Pitt, C. G.; Carey, R. N.; Toren, E. C. *J. Am. Chem. Soc.* **1972**, *94*, 3806. (d) Pitt, C. G.; Bursey, M. M.; Rogerson, P. F. *J. Am. Chem. Soc.* **1970**, *92*, 519. (e) Bock, H.; Ensslin, W. *Angew. Chem., Int. Ed. Engl.* **1971**, *10*, 404. (f) Cowley, A. H.; Dewar, M. J. S.; Goodman, D. W.; Padolina, M. C. *J. Am. Chem. Soc.* **1974**, *96*, 2648. (g) Cowley, A. H. In *Homoatomic Rings, Chains and Macromolecules of Main Group Elements*; Rheingold, A. L., Ed.; Elsevier: Amsterdam, The Netherlands, 1977.
(6) (a) Zeigler, J. M.; Harrah, L. A.; Johnson, A. W. *Polym. Prepr. (Am. Chem. Soc., Div. Polym. Chem.)* **1985**, *26*, 345; *SPIE Adv. Resist. Technol. Proc. II* **1985**, *539*, 166. (b) Kepler, R. G.; Zeigler, J. M.; Harrah, L. A. *Bull. Am. Phys. Soc.* **1984**, *29*, 509. (c) Hofer, D. C.; Miller, R. D.; Willson, C. G. *SPIE Adv. Resist. Technol. Proc. II* **1984**, *469*, 16. (d) Harrah, L. A.; Zeigler, J. M. *Abstracts of Papers*, International Congress of Pacific Basin Chemical Societies, Honolulu, HI, American Chemical Society: Washington, DC, 1984; Abstract 09F0016. (e) Hofer, D. C.; Miller, R. D.; Willson, C. G.; Neureuther, A. *SPIE Adv. Resist. Technol. Proc. II* **1984**, *469*, 108.

0002-7863/88/1510-4522$01.50/0

Table III. Si_2H_6 EPT/6-31G(2d) Vertical Ionization Energies (eV)

	Koopmans	EPT(2)	EPT(3)	EPT(OVA)	exptl[5a,b]
$^2A_{1g}$	11.00	10.33	10.35	10.40	10.53
^2E_g	12.90	12.01	11.97	12.04	11.9, 12.1
^2E_u	13.64	12.76	12.73	12.80	12.73, 13.08

Table IV. Si_2H_6 EPT/6-31G** Vertical Ionization Energies (eV)

	Koopmans	EPT(2)	EPT(3)	EPT(OVA)	exptl[5a,b]
$^2A_{1g}$	10.96	10.33	10.38	10.43	10.53
^2E_g	12.85	12.12	12.11	12.21	11.9, 12.1
^2E_u	13.59	12.85	12.85	12.94	12.73, 13.08

Table V. Si_2H_6 EPT/6-31G(2d,p) Vertical Ionization Energies (eV)

	Koopmans	EPT(2)	EPT(3)	EPT(OVA)	exptl[5a,b]
$^2A_{1g}$	10.97	10.36	10.46	10.51	10.53
^2E_g	12.87	12.13	12.15	12.25	11.9, 12.1
^2E_u	13.61	12.86	12.89	12.98	12.73, 13.08

Poles of the matrix **G** are electron binding energies. The matrices are expressed in the canonical molecular orbital (MO) basis, so that

$$\{\mathbf{G}_0^{-1}(E)\}_{ij} = (E - \epsilon_i)\delta_{ij}$$

In the above equation, the ϵ's are canonical MO energies. The diagonality of the matrix $\mathbf{G}_0$ shows that its poles occur at these values; in other words, the neglect of $\sum E$ leads to Koopmans's theorem. The present EPT calculations are carried out in the quasi-particle approximation; i.e., a single, diagonal element of the self-energy matrix is needed for each final state. An iterative pole search at the second-order level (EPT(2)) is performed; this energy is then inserted into the third-order (EPT(3)) self-energy formula.[17] The diagrams evaluated in this way are then used to calculate the outer-valence approximation (OVA) to higher order corrections.[18] Only core MO's are omitted from the diagram summations. SCF calculations are performed with the CRAY-COS version of GAUSSIAN 82.[19] The EPT codes are a separate link to this suite of programs and employ many of the post-SCF utility subroutines of GAUSSIAN 82. Because this scheme issues from a closed-shell reference, no spin contamination occurs in either the neutral initial state or the cationic final state. This treatment of vertical electron binding energies has proven effective for the outer-valence ionization energies of ordinary molecules, van der Waals complexes, and molecular anions.[20]

Table VI. Si_3H_8 HF/3-21G* Geometry, C_{2v} Symmetry

Bond Lengths (Å)	
Si–Si	2.345
Si1–H	1.477 (H's in Si plane)
Si1–H	1.478 (H's out of Si plane)
Si2–H	1.480
Bond Angles (deg)	
Si-Si-Si	111.1
Si2–Si1–H	111.2 (H's in Si plane)
Si2–Si1–H	109.8 (H's out of Si plane)
Si1–Si2–H	109.4
Dihedral Angle (deg)	
Si–Si–Si–H	59.5 (H's out of Si plane)

Total Energy: −867.073 55 au

Table VII. Si_3H_8 EPT/6-31G* Vertical Ionization Energies (eV)

	Koopmans	EPT(2)	EPT(3)	EPT(OVA)	exptl[5a,b]
$^2B_2$	10.45	9.69	9.70	9.73	9.87
$^2A_1$	11.48	10.57	10.57	10.61	10.72
$^2B_1$	12.77	11.75	11.70	11.78	11.65
$^2A_2$	13.19	12.24	12.19	12.26	12.02, 12.17

III. Disilane

Because the ground state of disilane has been studied extensively by other workers,[10] this section primarily will assess the reliability of various EPT treatments of vertical ionization energies. (HF/3-21G* structure optimizations on the staggered D_{3d} form agree with ref 10b and are close to the electron diffraction results of ref 21.) The first basis set employed is 6-31G*. Table I shows that these results are quite satisfactorily for the ^2A_g, ^2E_g, and ^2E_u final states. Note that second order contains most of the needed corrections to Koopmans's theorem results. Third-order and OVA results differ little from the second-order results; such small differences suggest that further improvements in the self-energy treatment of relaxation and correlation corrections will be minor. To test whether these results are merely a fortuitous cancellation of basis set and self-energy errors, the calculations are repeated with larger basis sets.[11] Tables II–IV show EPT results when the 6-31+G*, 6-31G(2d), and 6-31G** basis sets are employed. All three of these sets constitute incremental improvements: diffuse s and p functions on the Si's, two sets of Si polarization functions instead of one, and polarization functions on the H's, respectively. In the first two cases the changes are inconsequential; the other case displays small, but noticeable, alterations. Therefore, the two most important basis augmentations are combined to give the

(7) (a) Herman, A.; Dreczewski, B.; Wojnowski, W. *Chem. Phys.* **1985**, *98*, 475. (b) Bigelow, R. W. *Chem. Phys. Lett.* **1986**, *126*, 63. (c) Bigelow, R. W.; McGrane, K. M. *J. Polym. Phys. B* **1986**, *24*, 1233. (d) Dewar, M. J. S; Lo, D. H.; Ramsden, C. A. *J. Am. Chem. Soc.* **1975**, *97*, 1311. (e) Gordon, M. S.; Neubauer, L. *J. Am. Chem. Soc.* **1974**, *96*, 5690. (f) Verwoerd, W. S. *J. Comput. Chem.* **1982**, *3*, 445. (g) Dewar, M. J. S.; Caoxian, J. *Organometallics* **1987**, *6*, 1486. (h) Bigelow, R. W. *Organometallics* **1986**, *5*, 1502.

(8) (a) Takeda, K.; Matsumoto, N.; Fukuchi, M. *Phys. Rev. B* **1984**, *30*, 5871. (b) Takeda, K.; Teramae, H.; Matsumoto, N. *J. Am. Chem. Soc.* **1986**, *108*, 8186. (c) Klingensmith, K. K.; Downing, J. W.; Miller, R. D.; Michl, J. *J. Am. Chem. Soc.* **1986**, *108*, 7438. (d) Teramae, H.; Yamabe, T. *Theor. Chim. Acta* **1983**, *64*, 1.

(9) (a) Damewood, J. R.; West, R. *Macromolecules* **1985**, *18*, 158. (b) Damewood, J. R. *Macromolecules* **1985**, *18*, 1793. (c) Hummel, J. P.; Stackhouse, J.; Mislow, K. *Tetrahedron* **1977**, *33*, 1925. (d) Hoenig, H.; Hassler, K. *Monatsh. Chem.* **1982**, *113*, 129.

(10) (a) Nicholas, G.; Berthelat, J. C.; Durand, P. *J. Am. Chem. Soc.* **1976**, *98*, 1346. (b) Luke, B. T.; Pople, J. A.; Krogh-Jespersen, M. B.; Apeloig, Y.; Chandrasekhar, J.; Schleyer, P. v. R. *J. Am. Chem. Soc.* **1986**, *108* 260. (c) Halevi, E. A.; Winkelhofer, G.; Meisl, M.; Janoschek, R. *J. Organomet. Chem.* **1985**, *294*, 151. (d) Berkovitch-Yellin, Z.; Ellis, D. E.; Ratner, M. A. *Chem. Phys.* **1981**, *62*, 21. (e) Blustin, P. H. *J. Organomet. Chem.* **1976**, *105*, 161. (f) Topiol, S.; Ratner, M. A.; Moskowitz, J. W. *Chem. Phys.* **1977**, *20*, 1. (g) Collins, J. B.; Schleyer, P. v. R.; Binkley, J. S.; Pople, J. A. *J. Chem. Phys.* **1976**, *64*, 5142. (h) Snyder, L. C.; Wasserman, Z. *Chem. Phys. Lett.* **1977**, *51*, 349. (i) Sax, A. F. *J. Comput. Chem.* **1985**, *6*, 469.

(11) (a) 3-21G*: Pietro, W. J.; Francl, M. M.; Hehre, W. J.; DeFrees, D. J.; Pople, J. A.; Binkley, J. S. *J. Am. Chem. Soc.* **1982**, *104*, 5039. Gordon, M. S.; Binkley, J. S.; Pople, J. A.; Pietro, W. J.; Hehre, W. J. *J. Am. Chem. Soc.* **1982**, *104*, 2797. Binkley, J. S.; Pople, J. A.; Hehre, W. J. *J. Am. Chem. Soc.* **1980**, *102*, 939. (b) 6-31G*: Hehre, W. J.; Ditchfield, R.; Pople, J. A. *J. Chem. Phys.* **1972**, *56*, 2257. Francl, M. M.; Pietro, W. J.; Hehre, W. J.; Binkley, J. S.; Gordon, M. S.; DeFrees, D. J.; Pople, J. A. *J. Chem. Phys.* **1982**, *77*, 3654. Hariharan, P. C.; Pople, J. A. *Theor. Chim. Acta* **1973**, *28*, 213. (c) 6-31G(2d): Frisch, M. J.; Pople, J. A.; Binkley, J. S. *J. Chem. Phys.* **1984**, *80*, 3265. (d) 6-31+G* (diffuse functions): Clark, T.; Chandrasekhar, J.; Spitznagel, G. W.; Schleyer, P. v. R. *J. Comput. Chem.* **1983**, *4*, 294.

(12) Hartree–Fock geometry optimizations with triple-ζ basis sets, p functions on H nuclei, and double-polarization functions on Si do not give significantly different results from the double-ζ plus polarization on Si treatment.

(13) MBPT(2) stands for second-order many-body perturbation theory, which is also known by the Hamiltonian partitioning scheme it employs: Møller–Plesset. Bartlett, R. *Annu. Rev. Phys. Chem.* **1981**, *32*, 359; Binkley, J. S. Pople, J. A. *Int. J. Quantum Chem.* **1975**, *9*, 229.

(14) (a) von Niessen, W.; Schirmer, J.; Cederbaum, L. S. *Comput. Phys. Rep.* **1984**, *1*, 57. (b) Herman, M. F.; Freed, K. F.; Yeager, D. L. *Adv. Chem. Phys.* **1981**, *48*, 1. (c) Ohrn, Y.; Born, G. *Adv. Quantum Chem.* **1981**, *13*, 1. (d) Simons, J. *Theoretical Chemistry: Advances and Perspectives*; Eyring, H., Ed.; Academic: New York, 1978; Vol. 3.

(15) Koopmans, T. *Physica (Amsterdam)* **1934**, *1*, 104.

(16) Ortiz, J. V. Ph.D. Dissertation, University of Florida, Gainesville, FL, 1981.

(17) For these electron binding energies, the derivative of the inverse Green's function with respect to E is low in second order. Changes in third-order results with different E's are expected to be small.

(18) Cederbaum, L. S.; Domcke, N.; von Niessen, W. *J. Phys. B* **1977**, *10*, 2963.

(19) GAUSSIAN 82: Release A by J. S. Binkley, D. DeFrees, M. Frisch, E. Fluder, J. A. Pople, K. Ragavachari, H. B. Schlegel, R. Seeger, R. Whiteside, Carnegie Mellon University, Pittsburgh, PA.

(20) Ortiz, J. V. *J. Chem. Phys.* **1987**, *86*, 308. Ortiz, J. V. *Chem. Phys. Lett.* **1987**, *134*, 366. Ortiz, J. V. *Chem. Phys. Lett.* **1987**, *136*, 387. Ortiz, J. V. *J. Chem. Phys.* **1987**, *87*, 1701. Ortiz, J. V. *J. Am. Chem. Soc.* **1987**, *109*, 5072. Ortiz, J. V. *J. Chem. Phys.* **1987**, *87*, 3557.

(21) Beagley, B.; Conrad, A. R.; Freeman, J. M.; Monaghan, J. J.; Norton, B. G.; Holywell, G. C. *J. Mol. Struct.* **1972**, *11*, 371.

6-31G(2d,p) results of Table V. The rapid convergence of theory with respect to basis set and self-energy improvements implies that these computational models are reliable for related systems.

Quasi-particle EPT calculations are compatible with the molecular orbital description of one-electron wave functions.[16] The MO corresponding to the cation ground state belongs to the totally symmetric irreducible representation. Each Si has a p orbital pointing toward the opposite Si in a σ bonding relationship. p orbitals perpendicular to the Si–Si bond occur in the next two MO's. These p orbitals are in a bonding relationship with the s orbitals on the H's. For the e_g and e_u MO's, the Si p's are Si–Si antibonding and bonding, respectively. The primary function of these two sets of degenerate MO's is Si–H bonding. Lower MO's are dominated by 3s contributions from the Si's and contribute to the inner-valence region of the photoelectron spectrum.

An inspection of the experimental spectrum[5a,b] shows that the maxima referenced in Tables I–V belong to broad features. The half-width at half-height is a few tenths of an electronvolt for the first peak centered about 10.53 eV. Because the final-state vacancy corresponds to a highly bonding MO, much vibrational structure is probably hidden under this broad feature. Ionizations corresponding to the next two pairs of degenerate levels should exhibit Jahn–Teller final-state splittings. The maxima at 11.9 and 12.1 eV also belong to a broad feature. The next two maxima, at 12.73 and 13.08 eV, are considerably sharper and bracket the EPT(OVA)/6-31G(2d,p) result. The converged theoretical results coincide reasonably well with the experimental disilane maxima. The simplest basis, 6-31G*, provides sufficiently accurate results to be useful in studying larger silane chains.

IV. Trisilane

EPT calculations at the Hartree–Fock, 3-21G* optimum geometry (Table VI) are performed with the 6-31G* basis. (This treatment is called EPT/6-31G*//HF/3-21G*.) The C_{2v} structure has staggered dihedral angles, so there are three pairs of symmetry-related H nuclei above and below the plane defined by the three Si nuclei and two H's that lie in this plane. Results for four final cation states are summarized in Table VII. Once again, the OVA third-order and second-order results agree closely. The two highest MO's are dominated by bonding relationships between adjacent Si's. By symmetry, the b_2 highest occupied MO in the Si1–Si2 bonding region has the opposite phase as that in the Si2–Si3 region. The a_1 MO is totally symmetric, so that these two regions have the same phase in this orbital. The b_1 and a_2 MO's are more localized in the Si–H bonding regions above and below the plane containing the three Si's.

The two lowest experimental ionization energies[5a,b] referenced in Table VII belong to features with sharpness comparable to that of the lowest energy peak in the disilane spectrum. The two peaks partially overlap but are clearly distinguishable. The next peak, at 11.65 eV, is located on the shoulder of a large, broad feature that corresponds to MO's with Si–H bonding character. Near the top of this same feature lie two peaks at 12.02 and 12.17 eV. Other local maxima lie at 12.8 and 13.02 eV. The existence of a large, broad feature at energies higher than the smaller peaks' energies is common to both disilane and trisilane. The latter are relatively sharp because the vertical ionization energy separations are large for the Si–Si bonding levels. Separations of the Si–H bonding levels are not as great, and a broad feature results. Agreement with experiment is good for trisilane, with the calculated vertical ionization energies lying within 0.1 or 0.2 eV of the observed maxima.

V. Normal Tetrasilane

With tetrasilane, the existence of two stable minima becomes a consideration. HF/3-21G* geometry optimizations are performed on the anti (C_{2h}) and gauche (C_2) isomers. Because barriers to rotations are important in understanding interconversions between these rotamers, two eclipsed conformers are optimized. The first of these, where the dihedral angle between the Si1–Si2–Si3 and Si2–Si3–Si4 planes is zero, is denoted ecl-0 and has C_{2v} symmetry. The other, where this dihedral angle is fixed at 120°, is denoted ecl-120 and has C_2 symmetry. The sequence anti, ecl-120, gauche, and ecl-0 describes a steady decrease of the dihedral angle from 180° to 120° to 60° to 0°. A reoptimization of this dihedral angle for the gauche minimum shows only trivial deviations from 60°. Tables VIII–XI summarize the findings of these optimizations. A slight elongation occurs for the central Si–Si bond of the eclipsed rotamers. The Si–Si–Si angle increases slightly in the ecl-0 structure. The bond angles stay close to tetrahedral values and the dihedral angles, when not constrained by symmetry, are near to 60°, −60°, and 180°. The changes with respect to Si–Si and Si–H bond lengths and to Si–Si–H and Si–Si–Si bond angles in disilane and trisilane are very small, implying that using a standard set of these values for larger silane chains is a reasonable approximation.

Hartree–Fock and MBPT(2) calculations with the 6-31G* basis are performed at these geometries. Relative energies in Table XII show that the energy difference between the two minima is quite small. This conclusion is consistent at all three approximations listed. So small is this difference that present methods are unable to decide which is lower. The most advanced of the present calculations, with correlation corrections and a polarized

Table VIII. Anti Si_4H_{10} HF/3-21G* Geometry, C_{2h} Symmetry

Bond Lengths (Å)	
Si1–Si2	2.344
Si2–Si3	2.348
Si1–H	1.477 (H's in Si plane)
Si1–H	1.477 (H's out of Si plane)
Si2–H	1.481
Bond Angles (deg)	
Si–Si–Si	111.7
Si2–Si1–H	111.2 (H's in Si plane)
Si2–Si1–H	109.8 (H's out of Si plane)
Si1–Si2–H	109.7
Dihedral Angles (deg)	
Si3–Si2–Si1–H	59.6 (H's out of Si plane)
Si1–Si2–Si3–H	59.0

Total Energy: −1155.719 87 au

Table IX. Gauche Si_4H_{10} HF/3-21G* Geometry, C_2 Symmetry

Bond Lengths (Å)	
Si1–Si2	2.345
Si2–Si3	2.347
Si1–H	1.477, 1.477, 1.478
Si2–H	1.480, 1.480
Bond Angles (deg)	
Si–Si–Si	111.5
Si2–Si1–H	110.9, 110.1, 109.8
Si1–Si2–H	108.9, 109.5
Dihedral Angles (deg)	
Si3–Si2–Si1–H	179.9, 59.3, −59.9
Si1–Si2–Si3–H	59.8, 58.2

Total Energy: −1155.719 60 au

Table X. Ecl-0 Si_4H_{10} HF/3-21G* Geometry, C_{2v} Symmetry

Bond Lengths (Å)	
Si1–Si2	2.345
Si2–Si3	2.359
Si1–H	1.477 (H's in Si plane)
Si1–H	1.477 (H's out of Si plane)
Si2–H	1.480
Bond Angles (deg)	
Si–Si–Si	112.8
Si2–Si1–H	110.8 (H's in Si plane)
Si2–Si1–H	110.0 (H's out of Si plane)
Si1–Si2–H	108.8
Dihedral Angles (deg)	
Si3–Si2–Si1–H	59.6 (H's out of Si plane)
Si1–Si2–Si3–H	58.7

Total Energy: −1 155.717 86 au

Table XI. Ecl-120 Si_4H_{10} HF/3-21G* Geometry, C_2 Symmetry

Bond Lengths (Å)	
Si1–Si2	2.343
Si2–Si3	2.357
Si1–H	1.477, 1.477, 1.478
Si2–H	1.481, 1.480
Bond Angles (deg)	
Si–Si–Si	111.2
Si2–Si1–H	111.3, 109.7, 109.8
Si1–Si2–H	109.3, 109.7
Dihedral Angles (deg)	
Si3–Si2–Si1–H	180.0, 59.6, −59.5
Si1–Si2–Si3–H	59.1, 58.6
Total Energy: −1155.71868 au	

Table XII. Relative Energies of Si_4H_{10} HF/3-21G* Structures (eV)

	HF/3-21G*	HF/6-31G*	MBPT(2)/6-31G*
anti	0.000	0.000	0.000
gauche	0.007	0.008	−0.002
ecl-0	0.055	0.072	0.054
ecl-120	0.032	0.027	0.025

Table XIII. Anti Si_4H_{10} EPT/6-31G* Vertical Ionization Energies (eV)

	Koopmans	EPT(2)	EPT(3)	EPT(OVA)
^2A_g	10.03	9.23	9.25	9.27
^2A_g	11.42	10.40	10.42	10.46
^2B_u	11.60	10.67	10.69	10.73
^2B_g	12.73	11.62	11.60	11.67
^2A_u	12.97	11.94	11.90	11.97

Table XIV. Gauche Si_4H_{10} EPT/6-31G* Vertical Ionization Energies (eV)

	Koopmans	EPT(2)	EPT(3)	EPT(OVA)
^2A	10.26	9.44	9.48	9.49
^2B	10.90	10.00	10.01	10.05
^2A	11.77	10.74	10.76	10.81
^2A	12.92	11.82	11.80	11.87
^2B	12.92	11.88	11.85	11.92

basis, says that the gauche form is lower than the anti form by 0.04 kcal/mol; the Hartree–Fock prediction with the same basis gives anti as more stable by 0.19 kcal/mol. Small barriers separate the anti and the two gauche forms. The barrier between anti and gauche (ecl-120) is somewhat smaller than the barrier between the two gauche forms (ecl-0). MBPT(2)/6-31G*//HF/3-21G* calculations, listed in the last row of Table XII, give 0.58 kcal/mol for the former barrier and 1.25 kcal/mol for the latter. This result is consistent with the larger stretch of the central Si–Si bond and the larger opening of the Si–Si–Si angle in the optimzed ecl-0 structure versus the ecl-120 structure. The present results imply that steric factors will dominate considerations of the relative energies of substituted rotamers as there is little electronic bias in favor of either form. (Nonbonded repulsions between H's are also present in these calculations, but they will be small compared to repulsions between large alkyl or aryl groups.) This is also in qualitative agreement with NMR broadening noted in decamethyltetrasilane.[2d,e] For decamethyl-substituted systems, the anti form is favored over the gauche form for steric reasons.

EPT/6-31G*//HF/3-21G* calculations are performed on all four structures. Results are given in Tables XIII–XVI for five final states. Once again, little disparity arises between the results after Koopmans's theorem results. Arrangement of the OVA results in a Walsh diagram (Figure 1) shows how vertical ionization energies vary with the Si–Si–Si–Si dihedral angle. The three highest levels correspond to MO's localized on the Si backbone. Two are symmetric with respect to C_2 rotation (the symmetry operation that is conserved for all four structures), and the other is antisymmetric. Both of the ^2A final-state curves rise

Table XV. Ecl-0 Si_4H_{10} EPT/6-31G* Vertical Ionization Energies (eV)

	Koopmans	EPT(2)	EPT(3)	EPT(OVA)
$^2A_1$	10.34	9.51	9.55	9.56
$^2B_2$	10.71	9.81	9.83	9.86
$^2A_1$	12.00	10.97	11.00	11.04
$^2A_2$	12.61	11.52	11.49	11.57
$^2B_1$	13.12	12.06	12.03	12.10

Table XVI. Ecl-120 Si_4H_{10} EPT/6-31G* Vertical Ionization Energies (eV)

	Koopmans	EPT(2)	EPT(3)	EPT(OVA)
^2A	10.09	9.29	9.32	9.33
^2B	11.31	10.38	10.41	10.44
^2A	11.53	10.51	10.53	10.57
^2B	12.81	11.73	11.70	11.78
^2A	12.97	11.93	11.89	11.97

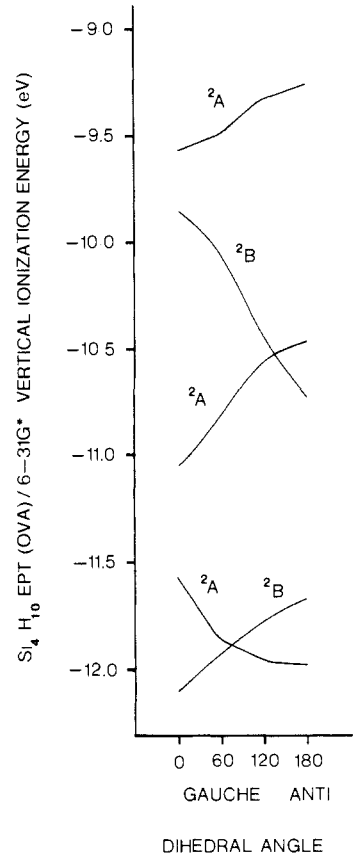

Figure 1. EPT(OVA)/6-31G* vertical ionization energies as a function of dihedral angle for Si_4H_{10}.

from left to right, but the ^2B curve declines sharply. The magnitudes of these changes are much greater than total energy changes for the ground states. Simple MO notions suffice to explain these trends. The ^2B curve belongs to an MO with a node between the central Si's. A bonding relationship holds in each Si1–Si2 region. Because of symmetry, these two bonding regions are out of phase with each other. These regions approach each other as one passes from right to left on the abscissa and the one-electron level is destabilized. The lower of the two symmetric MO's starts in the anti conformation as a bonding combination of Si2 and Si3 p orbitals pointing directly at each other. This level correlates to an MO with contributions from all four Si's in the ecl-0 case; this MO has no nodes between the Si's. The lack of any nodes in the backbone regions assures that this level will be the lowest of the Si–Si bonding orbitals. Increased delocalization in the ecl-0 case leads to stabilization as the nonadjacent Si–Si bonds approach. The last of the three belongs to the smallest vertical ionization energy. In the anti conformer, the

Table XVII. Anti-Anti Si_5H_{12} HF/3-21G* Geometry, C_{2v} Symmetry

Bond Lengths (Å)	
Si1–Si2	2.344
Si2–Si3	2.347
Si1–H	1.477 (H's in Si plane)
Si1–H	1.478 (H's out of Si plane)
Si2–H	1.480
Si3–H	1.481
Bond Angles (deg)	
Si–Si–Si	112.2 (interior)
Si–Si–Si	111.8 (exterior)
Si2–Si1–H	111.0 (H's in Si plane)
Si2–Si1–H	109.9 (H's out of Si plane)
Si3–Si2–H	109.0
Si2–Si3–H	109.3
Dihedral Angles (deg)	
Si3–Si2–Si1–H	59.6 (H's out of Si plane)
Si4–Si3–Si2–H	58.7
Total Energy: −1 444.366 19 au	

Table XVIII. Gauche-Gauche Si_5H_{12} HF/3-21G* Geometry, C_{2v} Symmetry

Bond Lengths (Å)	
Si1–Si2	2.344
Si2–Si3	2.348
Si1–H	1.477
Si2–H	1.481
Si3–H	1.481
Bond Angles (deg)	
Si–Si–Si	110.5 (interior)
Si–Si–Si	111.0 (exterior)
Si2–Si1–H	109.9, 109.8, 110.1
Si3–Si2–H	109.0, 110.1
Si2–Si3–H	109.0, 110.1
Dihedral Angles (deg)	
Si2–Si3–Si4–Si5	73.5
Si3–Si2–Si1–H	180.0, −59.6, 59.6
Si4–Si3–Si2–H	59.4, 58.9
Total Energy: −1 444.365 93 au	

Table XIX. Si_5H_{12} HF/3-21G* Canonical Orbital Energies (eV)

	anti–anti			gauche–gauche	
	energy	1–4 character		energy	1–4 character
2b	9.83	bonding	2b	10.18	bonding
2a	11.33	bonding	2a	10.74	antibonding
1a	11.54	antibonding	1b	11.34	antibonding
1b	11.74	antibonding	1a	11.92	bonding

electron density is primarily in the terminal Si–Si bonds. A bonding relationship exists in each Si1–Si2 region, and symmetry requires that these two regions be in phase with each other. This level must therefore have the opposite trend as the curve for the ^2B final state.

Because the total energies for anti and gauche are virtually the same, the photoelectron spectrum will probably depend on the vertical ionization energies of both isomers. Both the anti (9.27, 10.46, and 10.73 eV) and gauche (9.49, 10.05, and 10.81 eV) results are in reasonable agreement with the maxima[5a,b] at 9.62, 10.3, and 10.85 eV. In the Si–Si energy region, sufficiently many vertical ionization energies crowd into a small energy range to produce the broader features that are characteristic of the Si–H energy region in the smaller silanes. The gauche calculation agrees more closely with the observed maximum of lowest energy than does the anti calculation. We cannot distinguish whether a shoulder occurs at 9.3 eV from the data of ref 5a and 5b. In any case, the lowest calculated vertical anti ionization energy is contained within the experimental feature. The experimental curve is rather flat near the 10.3-eV local maximum, and both calculated second ionization energies are compatible with this maximum. The maximum at 10.85 eV is about as sharp as the one at 9.62 eV. Calculated values at 10.73 and 10.81 eV are close enough to explain this feature.

The energy difference between anti and gauche isomers will change as a result of ionization. For example, in ^2A final states, the anti form will be favored; ionizations from the gauche form will access excited vibrational levels. In the ^2B case, vertical ionizations from the anti isomer will be far away from the minimum of the potential energy surface. Interactions between nonadjacent Si–Si bonding regions are responsible for these effects. All three final states will have lost considerable bonding character between adjacent Si's as well. For these reasons, we expect a rich vibrational structure to be present under the broad envelopes of the experimental spectrum. In the Si–H energy region, maxima have been found[5a,b] at 11.6, 11.8, and 12.0 eV. The curves in Figure 1 for the two highest ionization energies suggest that both conformers contribute to these broad features as well. Two gauche vertical ionization energies lie near 11.8 eV, and the two highest anti vertical ionization energies lie near 11.6 and 12.0 eV.

On the basis of accurate EPT/6-31G*//HF/3-21G* calculations, both the anti and gauche forms apparently contribute to the observed spectrum. Calculations at this level are necessary to get quantitative agreement that leads to confident interpretation. Further studies of larger systems might require exploring the possibility of using less complicated methods. Inspection of the EPT results shows that second-order results are in excellent agreement with the third-order and OVA results; thus, this approximation might prove useful in introducing corrections to Koopmans's theorem. Quantitative errors in Koopmans's theorem are large, but the bonding trends are still useful. Curves parallel to those of Figure 1 are produced with Koopmans's theorem results, even with the 3-21G* basis. The main flaws of Koopmans's theorem results are the absolute energies and the relative displacements of the curves, but the dependence on dihedral angles is treated well.

VI. Normal Pentasilane

HF/3-21G* geometry optimizations are performed on the anti–anti and gauche–gauche conformers of the unbranched 5Si chain. The optimized structures have C_{2v} and C_2 symmetries, respectively. Tables XVII and XVIII show that bond lengths, angles, and dihedral angles do not vary much with an increase in chain length. The anti–anti form is lower in energy at this level by 0.007 eV (0.16 kcal/mol), but basis set and correlation improvements could reverse this order. This result is compatible with those of the previous section in that the two conformers have essentially the same energy.

As Koopmans's theorem results give a reasonable qualitative description of how vertical ionizations change with conformation in tetrasilane, the 3-21G* canonical orbital energies of pentasilane can perform a similar service in comparing the anti–anti and gauche–gauche conformers. The four highest occupied MO's are predominantly Si–Si nearest-neighbor σ bonding orbitals. Their symmetry labels and energies are listed in Table XIX for both conformers. (Note that classifications according to the C_2 rotation axis, a and b, apply to both cases and that, in the anti–anti C_{2v} conformer, the full point-group labels are a_1 and b_2.) In the anti–anti case, the lowest b level has a single node along the Si backbone at the central Si. This level correlates to a similarly constructed 1b level of the gauche–gauche conformer. The 1–4 interaction is antibonding, and so a destabilization of 0.40 eV results upon going from anti–anti to gauche–gauche, whereupon the nonadjacent bonds will be closer. The lowest a level of the anti–anti conformer is fully bonding along the backbone for the three central Si's, but the back lobes of the two Si2's, in bonding relationships with the end Si's, force the Si1–Si2 regions into the opposite phase. Therefore, Table XIX lists this level as 1–4 antibonding. The second a level of the anti–anti conformer is mostly concerned with Si1–Si2 bonding, but no nodes occur along the Si backbone. Even though this level has fewer nodes, the lack of interaction between the end bonds gives it a higher energy than the lower a level. For this reason the a MO which is 1–4 bonding is higher than the a MO which is 1–4 antibonding. When we move

to the gauche-gauche conformer, just the opposite occurs. The 1a level is the lowest of the four MO's and is 1-4 bonding. This level still emphasizes the central Si-Si bonds over the end Si-Si bonds. The 2a MO now has a node along the Si backbone at the Si2 positions and is therefore 1-4 antibonding. Neglecting the noncrossing rule temporarily, we note that the 1-4 bonding a level has fallen from -11.33 to -11.92 eV in going from anti-anti to gauche-gauche and that the 1-4 antibonding a level has risen from -11.54 to -10.74 eV. Because the 1-4 character in the two a levels reverses in energy order, an avoided crossing probably occurs in the middle of the process. We consider the 2b level, the highest occupied MO. In the anti-anti conformer, p orbitals aligned with the chain axis (i.e., perpendicular to the C_2 axis) along the Si backbone are in phase at every other Si position. Nearest neighbors have bonding relationships, but the Si1-Si2 and Si2-Si3 regions have opposite phase. This arrangement is preserved in the gauche-gauche form. As this orbital has b symmetry, the end bond region will interact favorably with the nonadjacent interior bond region. A stabilization of 0.35 eV in the gauche-gauche conformer versus the anti-anti conformer results.

As the chain length increases, the highest occupied MO will retain its bonding Si-Si nearest-neighbor quality and the out of phase relationship between adjacent bonding regions, implying that the 1-4 interactions will be in phase. As rotations about Si-Si single bonds occur, the highest occupied MO will be stabilized in the gauche versus anti conformation. This is compatible with the notion that the excitation energies in the anti form are shifted toward the red relative to those in the gauche form,[2,3] but a more definitive study would examine the conformational dependence of electron affinities (where Koopmans' theorem results are questionable) and excitation energies.

VII. Summary

We have carried out geometry optimizations at the SCF level using a 3-21G* basis for the unbranched forms of disilane, trisilane, tetrasilane, and pentasilane. Vertical ionization energies on these species are in excellent agreement with experiment. Total energy results for tetrasilane suggest no significant energy difference between the anti and gauche conformers. The trends of the EPT vertical ionization energies are consistent with MO concepts based on interactions of next nearest neighbors in a bond orbital model. If these ideas for tetrasilane and pentasilane can be extrapolated to longer polysilane chains, then we would expect the highest occupied states of the Si backbone to be stabilized with an increasing gauche population.

Acknowledgment. We thank the Naval Research Laboratory Research Advisory Committee for a grant of computer time on the NRL Cray-XMP, which made this work possible. Drs. J. Ziegler and K. Schweizer of Sandia National Laboratory, Albuquerque, NM, provided the initial stimulus to J.V.O. to undertake this study. J.V.O. also thanks the American Society for Engineering Education for support during the performance of this work.

Registry No. Si_2H_6, 1590-87-0; Si_3H_8, 7783-26-8; Si_4H_{10}, 7783-29-1; Si_5H_{12}, 14868-53-2.

Conformational Studies by Dynamic NMR. 35.[1] Structure, Conformation, and Stereodynamics of Hindered Naphthylamines

D. Casarini,[2a] E. Foresti,[2b] L. Lunazzi,*[2a] and D. Macciantelli[2c]

Contribution from the Department of Organic Chemistry, University, Viale Risorgimento 4, 40136 Bologna, Italy, the Department "G. Ciamician", University, Bologna, Italy, and the I.Co.C.E.A. CNR, Ozzano E., Bologna, Italy. *Received August 4, 1987*

Abstract: The low-temperature ^1H and ^{13}C NMR spectra of a number of *N*-ethyl- and of *N*-isopropyl-*N*-alkyl-1-naphthylamines allowed the measurement of the interconversion barriers between the two twisted enantiomeric conformers. The free energies of activation increased substantially with the dimension of the N-alkyl groups (e.g., $\Delta G^{\ddagger}_{173}$ is 8.3 Kcal mol^{-1} when N-alkyl is a methyl group, and $\Delta G^{\ddagger}_{373}$ is 19.8$_5$ Kcal mol^{-1} when N-alkyl is a *tert*-butyl group in *N*-ethyl-*N*-alkyl-1-naphthylamines). Nuclear Overhauser enhancement (NOE) experiments confirmed that these molecules adopt a twist conformation and indicated that in *N*-methyl as well as in *N*-ethyl-*N*-isopropyl-1-naphthylamines the *N*-isopropyl moiety is closer to H-8 than to H-2. These results, obtained in solution, were confirmed by the X-ray investigation of an analogous derivative in the solid state. On the other hand, the less hindered secondary 1-naphthylamines turned out to be planar in solution (NOE experiments) as well as in the solid state (X-ray diffraction). Finally it was found that electron-releasing (e.g., $-NH_2$) and electron-attracting (e.g., $-NO_2$) substituents in position 4 increase and reduce, respectively, the interconversion barriers of the twisted tertiary 1-naphthylamines. As expected this trend is opposite to that reported in the case of planar *N*-methylanilines containing analogous substituents in position 4.

The 1-isomers of the *N*,*N*-dialkylnaphthylamines are sufficiently hindered as to have the dynamic plane containing the two alkyl groups and the rapidly inverting nitrogen atom significantly twisted with respect to the plane of the naphthalene ring. As a consequence, the torsional process that allows the interconversion between the pair of conformers indicated in Scheme I requires the passage through a transition state where the two planes become coplanar. On the contrary the less hindered 2-naphthylamines are known to have planar ground states and perpendicular transition states.[3,4]

Scheme I

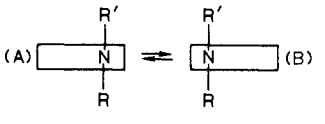

(1) Part 34. Casarini, D.; Lunazzi, L.; Macciantelli, D. *J. Org. Chem.* **1988**, *53*, 182-185.

(2) (a) Department of Organic Chemistry. (b) Department "G. Ciamician". (c) CNR, I.Co.C.E.A., Ozzano E.

0002-7863/88/1510-4527$01.50/0